APPLIED SCIENCES AND ENGINEERING

Modeling, design, and machine learning-based framework for optimal injectability of microparticle-based drug formulations

Morteza Sarmadi[1,2,3], Adam M. Behrens[2], Kevin J. McHugh[2], Hannah T. M. Contreras[2], Zachary L. Tochka[2], Xueguang Lu[2], Robert Langer[1,2,3]*, Ana Jaklenec[2]*

Inefficient injection of microparticles through conventional hypodermic needles can impose serious challenges on clinical translation of biopharmaceutical drugs and microparticle-based drug formulations. This study aims to determine the important factors affecting microparticle injectability and establish a predictive framework using computational fluid dynamics, design of experiments, and machine learning. A numerical multiphysics model was developed to examine microparticle flow and needle blockage in a syringe-needle system. Using experimental data, a simple empirical mathematical model was introduced. Results from injection experiments were subsequently incorporated into an artificial neural network to establish a predictive framework for injectability. Last, simulations and experimental results contributed to the design of a syringe that maximizes injectability in vitro and in vivo. The custom injection system enabled a sixfold increase in injectability of large microparticles compared to a commercial syringe. This study highlights the importance of the proposed framework for optimal injection of microparticle-based drugs by parenteral routes.

INTRODUCTION

Microencapsulation-based drug delivery has the potential to markedly improve drug efficacy, reduce toxicity, contribute to patient compliance and convenience, and even enable new therapies that may otherwise be infeasible to implement (*1*–*4*). Multiple designs and manufacturing techniques have been used to fabricate microparticles with a range of sizes and functionality (*5*–*9*), and various release kinetics can be obtained by modulating morphology, material composition, or active perturbation of the drug carrier (*4*–*11*). However, administration of microparticles and biomaterials via an injection holds several challenges (*12*–*18*). Depending on the application, the design of drug delivery systems may prioritize release kinetics, biocompatibility, or other factors that may conflict with optimal parameters used in parenteral injection, especially in subcutaneous administration (i.e., needle gauge, particle size, shape, and concentration) (*12*–*22*). Injectable microparticle formulations have been translated to the clinic for several controlled release drug applications (*12*, *23*). There are currently 11 U.S. Food and Drug Administration–approved microparticle-based drug formulations on the U.S. market (*23*). In addition, between 1980 and 2017, there have been 92 clinical trials globally and 45 clinical trials in the United States based on injectable microparticle formulations with a size ranging from 1 to 300 μm (*23*). High-efficiency transfer of microparticles through injection can play a key factor in delivering the correct dose to the patient and enable successful clinical translation of particulate drug delivery systems (*12*, *23*). As a result, there is a serious need for development of models and techniques providing insights into injection efficacy of any arbitrary microparticle system (*12*, *21*–*23*).

Despite major advances in drug encapsulation, there have been few reports on the investigation of injection efficacy. Hypodermic needles are the most accessible option for injection but can present a challenge for microparticle-based drug delivery because they can clog or retain particles in the syringe after injection is completed (Fig. 1). This study aims to establish a comprehensive framework for evaluating the delivery of a broad range of microparticles. We hypothesized that the percentage of microparticles that could be successfully transferred or injected to the patient would be a function of several different design elements (i.e., microparticle size, needle size, and viscosity of the injection solution). We then demonstrate the use of an integrated approach based on computational fluid dynamics (CFD), data science, and microfabrication techniques to address the issues related to microparticle administration.

To this end, we developed a multiphysics model, coupling CFD with microparticle transport to numerically analyze microparticle injectability in a syringe-needle system. This model was then used to explore the effect of different design elements such as microparticle shape, size, concentration, initial distribution, needle gauge (inner diameter), and viscosity of the injection solution on microparticle injectability. Experiments were then conducted to validate the numerical model. Two cycles of testing were performed using design of experiment (DOE) principles to study microparticle injectability and identify the importance of each design parameter. Results were then used to perform Taguchi analysis along with analysis of variance (ANOVA) to statistically identify the relative contribution of each design parameter. Subsequently, we demonstrated that two dimensionless parameters that use variables pertaining to properties of the microparticles, needle, and injection solution enable accurate prediction of injectability. An artificial neural network (ANN) was also trained and tested to further predict the injectability results along with the proposed formula. Next, using the resulting numerical and experimental understanding, a custom syringe was designed, manufactured, and tested in vitro and in vivo to improve injectability. Results of this study can aid in designing specific

[1]Department of Mechanical Engineering, Massachusetts Institute of Technology, Cambridge, MA 02139, USA. [2]David H. Koch Institute for Integrative Cancer Research, Massachusetts Institute of Technology, Cambridge, MA 02139, USA. [3]Harvard-MIT Division of Health Sciences and Technology, Institute for Medical Engineering and Science, Massachusetts Institute of Technology, Cambridge, MA 02139, USA.
*Corresponding author. Email: rlanger@mit.edu (R.L.); jaklenec@mit.edu (A.J.)

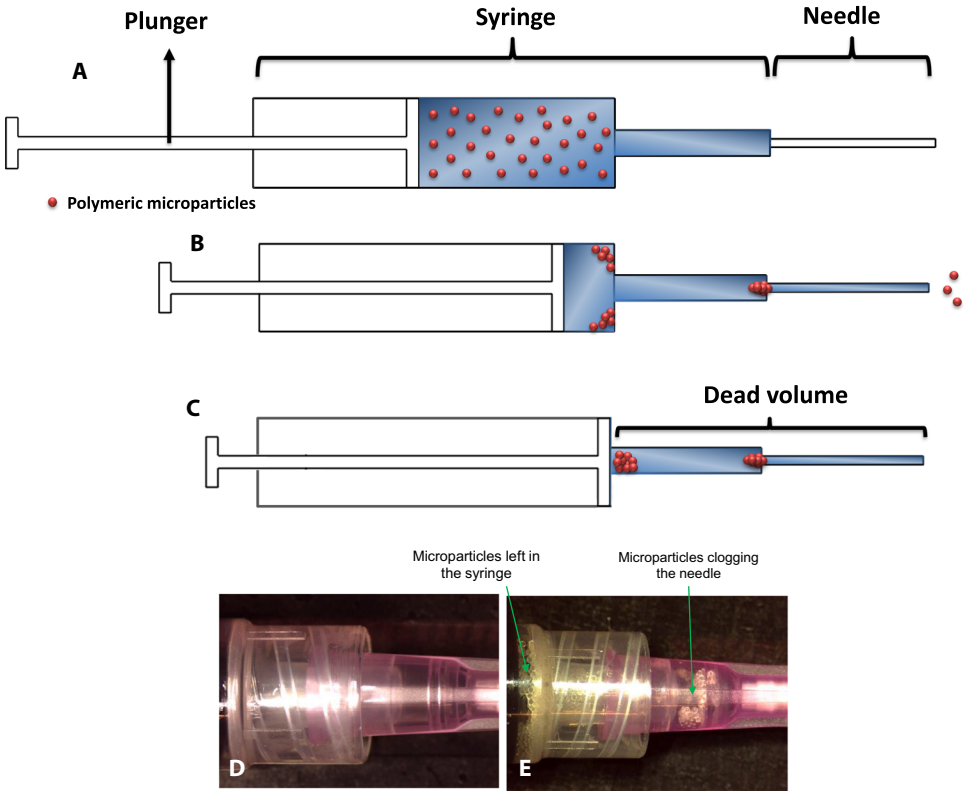

Fig. 1. Microparticle clog formation as a major barrier to administration of particulate biopharmaceutical formulations. Schematic illustration of a typical syringe attached to a hypodermic needle containing a homogenous mixture of polymeric microparticles (**A**) before injection, (**B**) during injection, and **(C)** after injection. The remaining volume of injection solution after full course of plunger in the syringe needle is called dead space or dead volume. Depending on different design elements, particles are not entirely transferred into the patient through the needle and they are prone to accumulate in the syringe or clog the needle. An experimental case of microparticle accumulation in the syringe and needle inlet in (**D**) empty syringe and (**E**) after the full course of plunger displacement. The system illustrated herein is a 3-ml-sized BD Luer-Lok syringe attached to an 18G BD hypodermic needle filled with a mixture of water/poly(lactic-co-glycolic acid) (PLGA). The microparticles are PLGA microspheres with average diameter of 325 μm. Photo credit: Morteza Sarmadi, Massachusetts Institute of Technology.

delivery systems, predict and prevent microparticle clog formation, and potentially improve delivery of microencapsulated drugs and injectable biomaterials.

RESULTS

Numerical evaluation

To gain a numerical perspective on the effect of design parameters (i.e., particle size, shape, concentration, distribution, needle gauge, and solution viscosity) on injectability, computational simulations were performed on a model 3-ml-sized syringe containing 2 ml of the injection solution (Fig. 2, A and B). These simulations revealed that the maximum flow velocity magnitude reached 5.7 mm/s in the syringe body (barrel) and increased almost 12 times in the syringe tip (70.5 mm/s) and 110 times (627 mm/s) inside the 18G needle (Fig. 2, C to E, and fig. S1). The velocity magnitude was equal to zero on the wall of the syringe needle, as expected for the no-slip boundary conditions. The resulting pressure contours also indicated that the syringe wall and plunger experienced the highest pressure value equal to 89 kPa. The pressure gradient generated at the flow inlet (plunger) was the driver for the Poiseuille flow throughout the syringe-needle system, leading to a parabolic velocity profile reaching its maximum value at the centerline. The gauge pressure decreased from its highest value (89 kPa) at the plunger to zero at the needle exit opening to atmosphere (fig. S1).

When using water as the injection solution, particle weight overcame the lateral drag force and the entire particle population sedimented, leading to zero injectability (Fig. 2, H and J). Within the range studied, viscosity was found to have a major impact on injectability. Injection with the low-viscosity solution [1% methylcellulose (MC), $\mu = 0.37$ Pa·s at inlet velocity of 2.88 mm/s] significantly enhanced particle transport compared to water, by close to 50 and 40% in 18G, and 21G needles, respectively. Nevertheless, further 2.5-fold increase in concentration of MC in the solution (2.5% MC, $\mu = 5.33$ Pa·s at inlet velocity of 2.88 mm/s) led to approximately only 20% of increase in injectability in both needles compared to 1% MC. A solution at an even higher viscosity (5% MC) was found to be hard to transfer to the syringe and impractical for injections.

The effects of other parameters (i.e., microparticle concentration, shape, and size) on injectability were then evaluated in the context of our model (Fig. 3 and fig. S2). Increasing concentration of particles in the solution decreased injectability in both needles (18G and 21G). Injectability of the smaller needle (21G) dropped almost twice that of the larger needle. Increasing particle concentration was found to be effective only after exceeding a certain concentration threshold (i.e., going from 500 to 800 particles per injection volume). Injectability of solutions loaded with 250 and 500 particles was almost identical and so was injectability of 800- and 1000-loaded particle solutions.

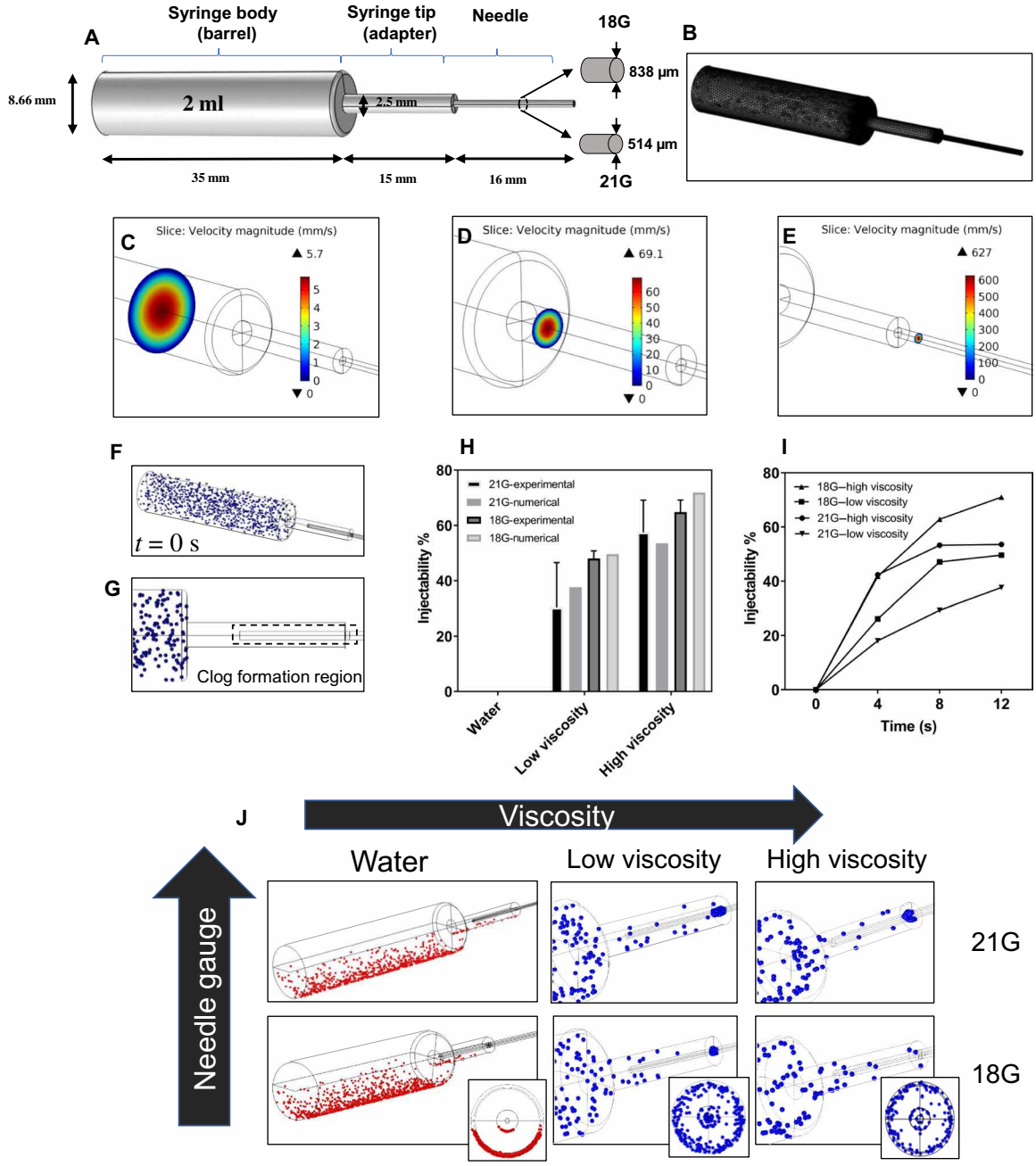

Fig. 2. Numerical modeling of clog formation in hypodermic syringe needles. (**A**) Illustration of the multiphysics numerical model used for simulations corresponding to geometry of a 3-ml-sized BD syringe containing 2 ml of particle-solution mixture. (**B**) Meshed geometry and velocity contours within different locations including (**C**) syringe body (barrel), (**D**) syringe tip (adapter), and (**E**) needle. (**F**) Initial position of particles in syringe barrel following random spatial distribution. (**G**) Critical location in the syringe needle defined before the needle inlet to incorporate clog formation domain in the numerical model. (**H**) A comparison between numerical and experimental values of injectability. (**I**) Injectability decreased over time as the microparticles clogged the needle. (**J**) Illustration of particles clogging the needle in the model for different needle gauges and injection solutions. Microspheres with an average diameter of 202 ± 6 µm and various concentrations were used in these simulations.

As expected, injectability decreased when larger microparticles were used, and a sharper decrease was observed in a 21G as compared to an 18G needle. In the 21G needle, increasing average particle diameter decreased injectability such that 200-µm particles yielded an injectability of just 35% compared to 71% for 50-µm particles. However, in the 18G needle, an increase in the average particle diameter from 50 to 200 µm decreased injectability slightly from 69 to 52%. These simulations further revealed that injectability depended on the needle size such that 18G needle in most cases had higher particle delivery than 21G needle (Fig. 2, H and I, and Fig. 3, A to C). Conversely, particle shape within the range studied did not independently influence the overall injectability.

The results of these simulations also demonstrated that concentrating particles in the centerline of the syringe body (smaller

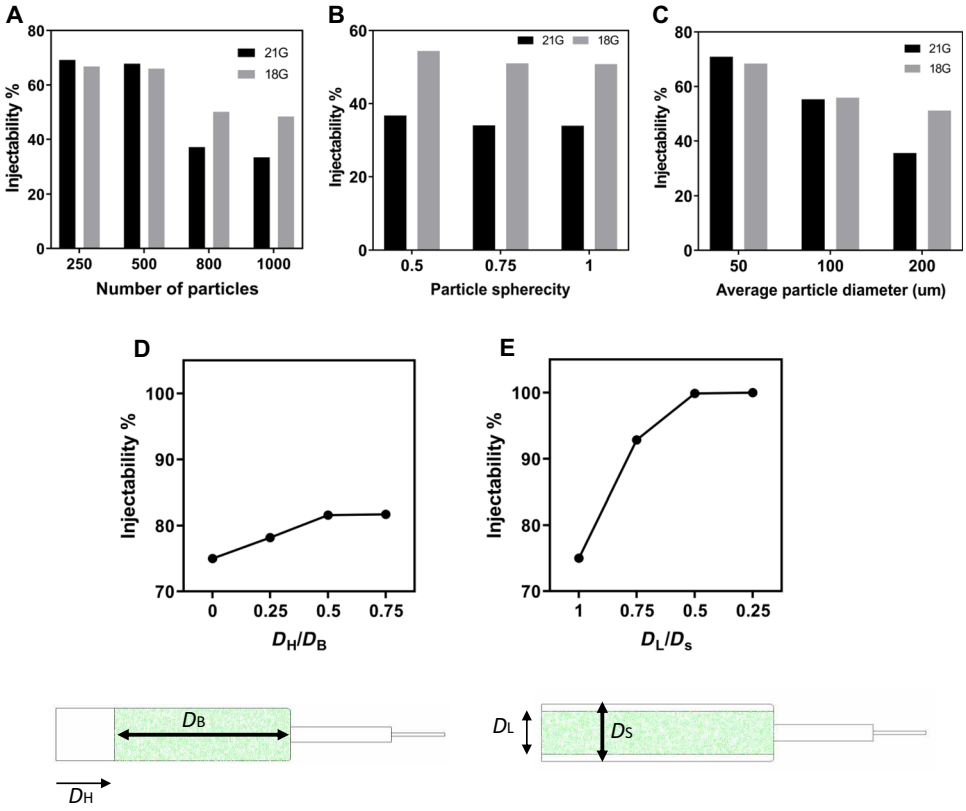

Fig. 3. Numerical results demonstrating the effect of design parameters important in drug delivery on microparticle injectability. (**A**) The effect of particle concentration (200 μm in diameter, spherical) on microparticle injectability. (**B**) Effect of particle sphericity (shape) on injectability. (**C**) Injectability of microspheres (1000 particles) as a function of particle size. Effect of initial particle offset (10,000 particles) from (**D**) the plunger and (**E**) the syringe inner wall on injectability. Particles are illustrated as green dots in the syringe.

D_L/D_S), closer to the regions with higher velocity magnitude, could enhance injectability (Fig. 3E and fig. S2). Shifting initial position of the particles toward the needle outlet (greater D_H/D_B) also increased injectability, reaching a plateau at $D_H/D_B = 0.5$. In agreement with the three-dimensional (3D) model, microparticles were found more likely to accumulate in the stagnation area located in the sharp corners of the syringe body that deviates from streamlines and represent recirculation of the velocity field away from the needle outlet. It was also observed that an offset distance from the wall, captured as the ratio D_L/D_S, represented a more pronounced effect on injectability than the offset distance from the plunger captured by D_H/D_B (Fig. 3, D and E, and fig. S2).

Experimental investigation

After implementing a numerical approach, we then sought to experimentally study injectability using a DOE approach. Injectability of a library of nine different micromolded particles with an approximate size range between 80 and 325 μm was studied with various shapes including cube, cylinder, and sphere (fig. S3 and table S1). To this end, two sets of experiments based on L_{18} Taguchi orthogonal array were designed and conducted for a 1-ml and a 3-ml syringe with different design factors/levels (tables S2 and S3).

The injectability values obtained from the DOEs are presented in Fig. 4 and table S3. In DOE1, the mean of injectability reached an approximate plateau at the low viscosity level (1% MC). Furthermore, while injection using a low-viscosity solution instead of water improved injectability by more than 50%, the difference between result of low- and high-viscosity solutions (1% MC, and 2.5% MC) was considerably less pronounced (less than 10%). In accordance with simulation results, increasing size of the microparticles decreased injectability for both syringe sizes studied. As also predicted by the simulations, the effect of microparticle size was more influential in injections using smaller needles (i.e., DOE2), as evident by a sharper decrease in injectability as a function of particle size.

A similar trend was observed for the effect of needle size, such that decreasing the needle size decreased injectability in agreement with the numerical results. Similar to particle size, the effect of the needle size was more pronounced in the context of the narrower needles used in DOE2 (needle inner diameters from 0.1 to 0.5 mm) compared to DOE1 (needle inner diameters from 0.5 to 1 mm). It was also observed that increasing particle concentration did not have a statistically significant effect within the range studied (approximately 30 to 150 particles in 300 μl). As predicted by the simulations, particle shape did not have a major effect on injectability. These trends were consistent between both syringe sizes.

Next, we used ANOVA based on a general linear model to identify the relative importance of each design factor on injectability (Fig. 4, G and H). Viscosity was found to be the most important parameter based on DOE1, offering a contribution percentage as high as 90% ($P < 0.0001$). By excluding viscosity as a variable and using narrower

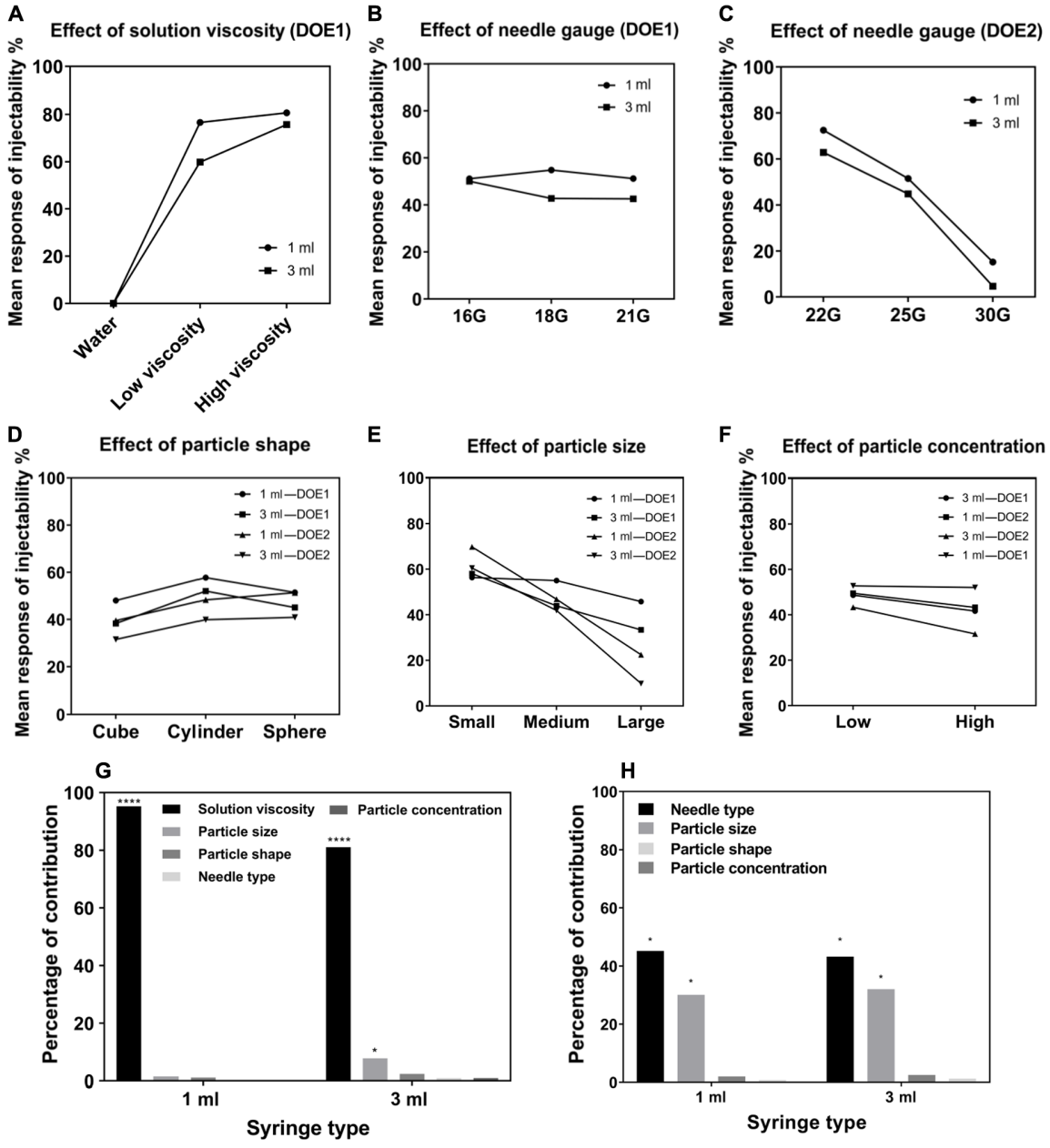

Fig. 4. Experimental study on the effect of different parameters on injectability. Mean response of injectability obtained from Taguchi analysis indicating the effect of the design parameters including (**A**) viscosity, (**B**) needle gauge (DOE1), (**C**) needle gauge (DOE2), (**D**) particle shape, (**E**) particle size, and (**F**) particle concentration. ANOVA results demonstrating the comparative significance and ranking of each of the design parameters studied for 1-ml and 3-ml syringes are shown (****$P < 0.0001$ and *$P < 0.05$). (**G**) From DOE1, solution viscosity was identified as the most important factor, and (H) in DOE2, needle size and particle size were the two dominant design parameters.

needles in DOE2, particle size and needle gauge became the two dominant design factors ($P < 0.05$), whereas the effect of particle concentration and shape was comparatively negligible.

Model development

Two dimensionless parameters (π_1 and π_2) were found to successfully predict the chance and range of injectability for various syringe-needle systems (see Materials and Methods). The first dimensionless parameter (π_1) was based on material properties and concentration of the particles and viscosity of the injection solution. The second dimensionless parameter represented the ratio of the needle diameter divided by the greatest dimension of the particle (π_2). The calculated injectability as a function of π_1 and π_2 was plotted to capture the parameter space necessary to yield high injectability region (Fig. 5, A and B).

A predicted injectability (denoted by *f*) of more than 60%, as the critical threshold, provided an actual injectability of at least 50%. The high injectability margin was further divided to two regions on the basis of the predicted injectability. Accordingly, the first case corresponded to a value of *f* equal to 60 to 85%, yielding an actual injectability of 72% on average. Second, an *f* value of 85% provided an average actual injectability of 85%. The criteria for choosing the

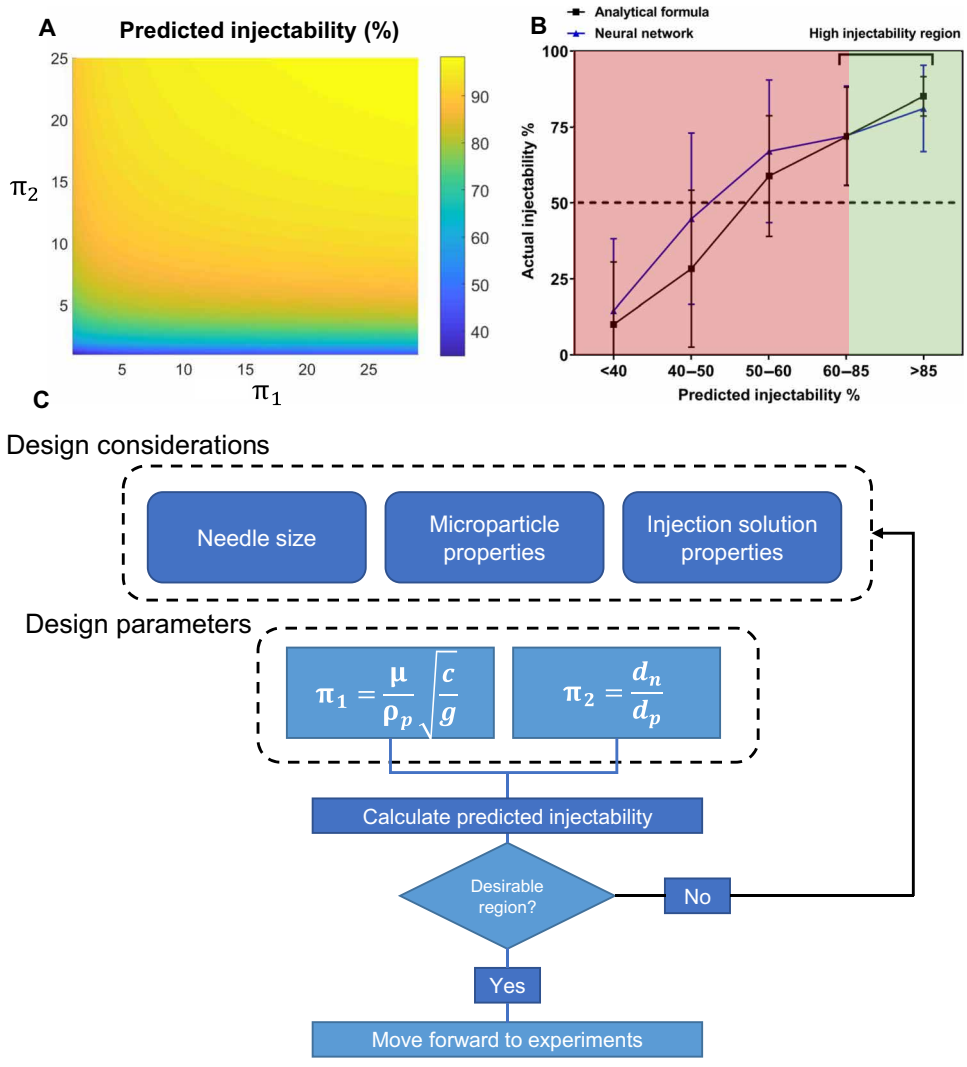

Fig. 5. Prediction of injectability for various syringe-needle systems. (**A**) The plot contour demonstrates predicted injectability as a function of the two nondimensional parameters calculated using Eq. 4. (**B**) The relationship between actual microparticle injectability from the experiments and the predicted injectability calculated by the formula and ANN. High injectability region was assumed where the lowest bound of actual injectability (average subtracted by standard deviation) was greater than 50%. Error bars show SD. (**C**) Proposed flowchart demonstrating the potential application of the proposed predictive tools for design of high injectability drug delivery microparticles.

high injectability margin were based on the needle dead volume (or dead space) (Fig. 1C). On the basis of the reported values in the literature, we considered the dead volume to be approximately between 25 and 30% for the injected volume in this study (*22*). An additional 22 experiments (n = 3) including both 1-ml and 3-ml syringes using microspheres made from polystyrene, poly(methyl methacrylate) (PMMA), and poly(lactic-co-glycolic acid) (PLGA) (table S4) were also performed to further validate the prediction formula. A comparison of actual injectability versus predicted injectability, f, is also presented in Fig. 5B. Pearson correlation coefficients of 0.84 and 0.79 were found between predicted and actual injectability in the sets of the DOEs and validation experiments, respectively. This finding suggests strong correlation between the predicted and actual injectability values.

Along with the proposed formula, an ANN was also trained for predicting microparticle injectability. The best training result corresponding to the lowest mean square error between the predicted and actual injectability values was achieved at epoch 63 (fig. S4). The trained ANN improved the overall R^2 value to 0.88 for the entire data population and to 0.90 for the testing data subset (fig. S4). Mapping of actual injectability to the predicted values obtained from the ANN predictions was also compared with the values from the formula (Fig. 5B). As shown, the simplified formula can provide reasonable accuracy resembling the results provided by the ANN. Both methods suggested that a predicted value of greater than 60% could be used as a high injectability margin, yielding an actual injectability of at least 50%. The workflow for using the proposed predictive injectability tools is also illustrated in Fig. 5C. A combined use of the proposed ANN and the formula can be used to predict injectability for a given microparticle morphology and only proceed to experiments where the predicted injectability falls within high injectability region ($f \geq 60\%$).

In line with numerical and experimental results, increasing viscosity from 0.001 to 1 Pa·s, considerably improved the predicted

injectability in both the proposed formula and the ANN. Increasing viscosity from 1 to 5 Pa·s did not have the same impact (fig. S4), which was also observed in the "Simulations" and "Experiments" sections. After converging to a certain value, particle concentration was found not to impose any major effect on predicted injectability for the present laminar regime. Furthermore, as expected, increasing the ratio of needle size to particle size (i.e., greater π_2) served to increase the predicted injectability.

Design of an optimized syringe geometry for improved injectability

We sought to use the resulting understanding of microparticle injectability to design and test a customized syringe design optimized for enhanced microparticle injectability. We studied injectability of cubic hollow and solid microparticles recently introduced as a promising platform for single-injection vaccine delivery, as an example (*5*). The results of the optimization and manufacturing of the proposed syringe, as well as the workflow summarizing these steps including numerical optimization, are provided in Fig. 6, A to D, and fig. S5.

In view of manufacturability and needle attachment considerations, a design ranked in the top 35% of 500 designs, numerically studied, was selected for a more comprehensive detailed design in SolidWorks and manufacturing (see the Supplementary Materials for more details regarding optimization procedure). In the detailed design step, we modified the typical geometry of a syringe and adopted a nozzle-shaped geometry in the syringe tip. This design was based on two interconnected nozzle geometries to increase velocity magnitude (hence, drag force on particles) at each nozzle outlet throughout the syringe tip. It was found that two design parameters had a major impact on microparticle transport: The slope of the syringe wall recapitulated by the angle θ, and the distance between barrel and syringe exit was denoted as L (Fig. 6D). The optimized syringe design provided a statistically significant improvement in the microparticle injectability compared to a similar 3-ml BD syringe as the control group (fig. S5). The custom syringe increased average injectability by 10 to 36%, showing greater improvement in injectability of particles with larger dimensions compared to a commercial syringe. A 1-ml version of the optimum 3-ml custom syringe was further manufactured and used for subcutaneous in vivo injection of cubic microparticles, as an example, to be covered next.

Injection of particles in vivo can be more challenging because of less control over parenteral injection parameters, in particular, in subcutaneous injection (e.g., angle of injection, flow rate, and position of syringe). High injectability in vivo plays an important step toward clinical translation of particle-based systems and drug delivery devices. To test our optimized syringe design, we performed injectability experiments in vivo in five animal models. We also evaluated different injection strategies, including modification to the initial distribution of particles before injection, inspired by the numerical results. The injection technique based on the combined use of the optimized syringe design and modified particle distribution provided the best result and significantly enhanced injectability of PLGA1 and PLGA2 (Fig. 6, H and I). In the case of PLGA1, it resulted in an approximately sixfold increase in injectability compared to injection using a conventional 1-ml syringe with homogeneously distributed particles. Moreover, a twofold increase was observed in injectability of PLGA2 using a combination of this combined approach compared to injecting particles with initial offset but without the proposed custom syringe.

As predicted by simulations, modifying particle distribution even without using the optimized syringe was found to be another method to increase injectability. Injections with particles positioned with an initial offset distance from the plunger increased the injectability of PLGA1 by a factor of 3.7 compared with homogenously distributed particles. Fabricating smaller microparticles (PLGA3) with the same cubic geometry also enhanced microparticle injectability. While injectability of PLGA3 dropped as the needle size decreased, a maximum injectability of 70% was achieved with an 18G needle (Fig. 6J). Furthermore, going from a 25G needle to an 18G needle led to 2.8-fold increase in injectability of PLGA3 particles.

DISCUSSION

While remarkable effort has gone toward the development of controlled release microparticle formulations, more resources are needed to better understand clinically viable administration using standard injectable methods. As the final step in administration of controlled release formulations, injection of microparticles could be a major hurdle toward clinical translation of microparticle-based (bio)pharmaceutical products (*12*). Numerical models coupled with statistical approaches have been widely implemented in design optimization of various engineering systems (*24*–*26*) and, more recently, used for biomedical applications (*27*–*34*). The used modeling approach of the clog formation criterion provided a novel method to address the barrier in current numerical software for simulation of adhesion of solid bodies, which could lead to numerical instabilities in conventional finite element software. It also enabled simulation of transport of a large number of solid particles interacting with the fluid, which could have been otherwise very difficult using a fluid-solid interaction approach.

Motivated by challenges associate with injection of microparticles, especially large microparticles, we aimed to systematically study microparticle transport through hypodermic needles. To this end, we initially developed a multiphysics finite element model coupling a CFD model of injection solution to transport of solid microparticles. Important design parameters affecting microparticle injectability were investigated using the developed model. We then proceeded with experiments to empirically examine the effect and significance of these design parameters on injectability. On the basis of the numerical and experimental findings, we proposed a model to predict chance of successful injection with a typical syringe-hypodermic device. Given poor performance of conventional syringe-needle devices for microparticle delivery, we finally proposed an optimized syringe design that provided significantly higher injectability for a vaccine delivery platform microparticle in vitro and in vivo.

Results showed that the particle size, needle size, and solution viscosity are the three most important design parameters (Figs. 2 to 4). Initial particle positioning in the syringe was another factor playing a major role in injectability (Fig. 3, D and E). While the role of particle concentration was found to be negligible, large polydispersity in particle size could potentially increase the chance of needle blockage for highly concentrated and polydisperse mixtures. Because transport of larger particles requires greater drag force and these particles have faster sedimentation velocity, they are more likely to get stuck in the syringe or clog the needle during injection. A more reliable approach in these cases could be considering the greatest dimension of the microparticle population as parameter d_p and selecting the needle gauge (d_n) accordingly. Increasing needle size will not always improve injectability, and the microparticle size relative to size of the

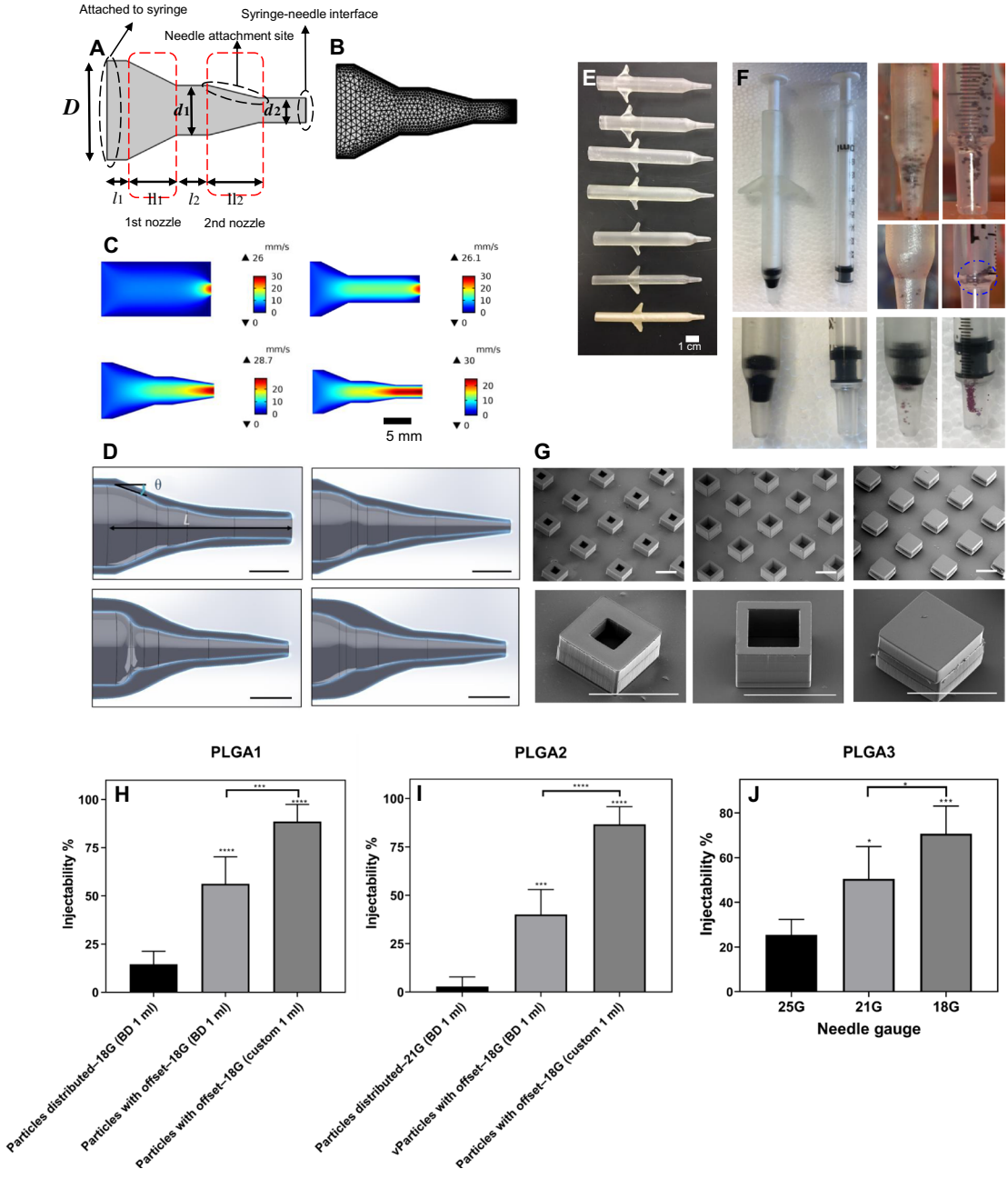

Fig. 6. Design, optimization, manufacturing, and in vivo testing of a customized syringe made for high injectability applications. (**A**) Design parameters considered in the numerical modeling and optimization of the syringe tip (adapter) based on two interconnected nozzles. (**B**) Meshed geometry of the syringe tip. (**C**) Velocity magnitude contour in some of the designs as the criterion for optimization. (**D**) Examples of detailed design of the syringe tip profile in SolidWorks based on different design parameters such as θ and *L*. Scale bars, 5 mm. (**E**) Different 3-ml-sized syringes (top five syringes) were manufactured by stereolithography (SLA) 3D printing to optimize needle attachment, decrease dead volume, and improve injectability in vitro. A 1-ml version of the optimum design (θ ~ 25°) based on in vitro injections was further manufactured for in vivo injections (two bottom designs). (**F**) Comparison between 1-ml version of the proposed syringe and a comparable commercial syringe. Unlike in the proposed design, particles were observed to accumulate in sharp corners in the barrel of the commercial syringe. The proposed design also demonstrated less dead volume accompanied by less particle waste. More details can be found in the Supplementary Materials. (**G**) Scanning electron microscopy (SEM) images of PLGA1-fabricated core-shell microparticles, a recently developed platform for single-injection vaccination. Different core geometries but the same exterior size (400 μm by 400 μm by 300 μm) can be achieved by modifying the manufacturing steps. Different configurations of the sealed and unsealed base layer in high and low magnifications are demonstrated. Scale bars, 500 μm. A full description of the manufacturing steps can be found in (*5*). (**H** to **J**) In vivo subcutaneous injection results ($n = 5$) using different strategies to enhance microparticle injectability (*$P < 0.05$, ***$P < 0.001$, and ****$P < 0.0001$). Particles were initially loaded into the syringe either randomly distributed (noted as "distributed") or with a certain offset from the plunger (noted as "with offset"). The term inside the brackets indicates type of the syringe, either the commercial or the proposed syringe. PLGA1, PLGA2, and PLGA3 refer to cubic particles with a dimension of 400 μm by 400 μm by 300 μm, 350 μm by 350 μm by 330 μm, and 162 μm by 162 μm by 162 μm made from PLGA(Resomer 502H), respectively. PLGA1 has a cubic internal core of 200 μm by 200 μm by 100 μm, while PLGA 2 and PLGA 3 are solid (i.e., nonhollow). Photo credit: Morteza Sarmadi, Massachusetts Institute of Technology.

needle should also be considered. From a clinical perspective, this approach is useful for obtaining an application-specific balance between allowable particle transfer and pain perception. It would therefore be important to find the minimum needle size that can provide the highest injectability for a given drug delivery application.

Solution viscosity was found to be a pivotal parameter for microparticle transport, consistent with the fact that increasing viscosity of a solution could substantially increase viscous drag forces on microparticles (Figs. 2 and 4). Notably, in the case of water, because of insufficient viscous drag forces (μ = 0.001 Pa·s), the density differential between polymer and water caused particles to sediment and zero injectability was observed. Two types of viscous drag force were therefore found to be essential for efficient microparticle injectability: longitudinal drag force, caused by the pressure-driven (Poiseuille) flow pushing particles toward the needle outlet, and lateral drag force resisting particle sedimentation (Fig. 2J). In more viscous solutions, both types of drag force increased; thus, higher driving forces were exerted on the particles along and across the syringe. The longitudinal viscous drag force contributed to particle transport toward the needle outlet, while the transverse drag force resisted particle sedimentation.

In a laminar regime, longitudinal viscous drag forces exerted on the particles are proportional to velocity magnitude and thus will decrease in locations where flow slows down. This can explain the reason for increased particle accumulation adjacent to syringe wall, as a result of no-slip boundary conditions, and sharp corners of the syringe corresponding to stagnation area. Viscous drag forces pushing particles forward in longitudinal direction would decrease in these areas. Moreover, in transition regions from barrel to syringe tip and from the syringe tip to needle inlet, a sharp decrease in the diameter could limit the number of particles that can effectively flow through a given cross section. As a result, locations associated with a decrease in diameter can be another critical domain with high risk of particle accumulation.

Unexpectedly, increasing viscosity did not always improve injectability. Increasing viscosity is accompanied by a decrease in Reynolds number, hence, an increase in Darcy's friction factor. As a result, increasing viscosity can also lead to higher head loss caused by increased viscous energy losses, making the flow of the injection solution through the syringe more difficult. Highly viscous solutions are also hard to transfer to the syringe. Increasing polymer concentration in solution beyond an optimum level will not always be productive. According to current study, a solution as viscous as 1% MC therefore can provide enough viscous drag forces to both transfer particles toward the needle outlet and prevent particle sedimentation. It can also be easily transferred and aspirated to the syringe. Furthermore, while high-viscosity solutions have been associated with less pain perception (*16*), they require higher injection pressure and larger needle gauges to accommodate syringability requirements (*15*, *16*). The downside of using larger needle diameters (smaller needle gauges) is greater pain perception at the injection site (*13*, *14*). Note that at a certain viscosity, negative influence of the increased viscous head loss could potentially outweigh improved drag force on the particles, preventing particle transport to the needle outlet.

Results further revealed that microparticle size, rather than concentration and shape, would play a major role in determining injectability (Figs. 3 and 4). Injecting a high number of small particles would impose lower risk of needle blockage compared to lower concentration of large particles. This finding also suggests that as long as particle size (more specifically, the greatest dimension of the microparticle) is conserved, various morphologies can essentially provide comparable injectability. As a result, by changing particle morphology but retaining particle size, a comparable injectability accompanied with a programmable release kinetics can be achieved. In this study, spherical particles with an average diameter of 50 μm, within the particle concentrations studied, were found easily injectable even with a 33G needle (d_n ~ 108 μm). Hence, we recommend this size as a good safety margin for injection of microencapsulated therapeutics through hypodermic needles.

The machine learning approach further supported the findings in injectability predictions and the DOE experiments (Fig. 5). Both machine learning– and Taguchi-based DOE have been widely used in pharmaceutics, health care, and biotechnology (*35*, *36*). The proposed ANN could be a more sophisticated tool for predicting injection efficacy. Notably, development of mathematical models as predictive tools for drug delivery efficacy has emerged as an area of active research (*2*, *11*). The trained machine learning script outputs a predicted injectability value for given values of π_1 and π_2 as the inputs. Specific conditions should be met for the proposed ANN and formula to be applicable. In general, we suggest these tools when π_2 is greater than 1 (preferably more than 2). In addition, particle size distribution is another factor that might elevate risk of particle clogging. We suggest considering the greatest particle size and dimension in a population of polydisperse particles when using these tools to consider a higher level of safety. In addition, it is recommended to calculate predicted injectability from both tools, find the converged values, and consider the lower one. The proposed framework refers to injections performed at a 0° angle of injection with particles randomly distributed in the barrel. At this angle, the entire component of the particle weight is perpendicular to the syringe axis and no additional component of particle weight can push particles toward the needle outlet.

On the basis of the proposed formula, the negative effect of using a solution with lower viscosity or particles with higher density (smaller π_1) can be partly compensated by using a greater d_n/d_p (higher π_2) (Fig. 5A). Increasing dimensions of the particles could be detrimental in two ways: (i) increasing sedimentation velocity and (ii) increasing risk of needle blockage. While injecting smaller particles could substantially increase microparticle injectability, manufacturing smaller microparticles might not always be feasible because of process challenges or release kinetics requirements. Notably, the plateau in the 2D contour (Fig. 5A and fig. S5) demonstrates that for a defined set of microparticle morphology and material properties (i.e., given π_1 and π_2), there would be a certain needle size at which maximum injectability could be attained. Increasing needle size beyond that level would not necessarily improve injectability, but it could adversely increase injection pain.

Last, the presented framework was adapted to facilitate microparticle delivery of a recently developed injectable biomaterial with a complex 3D structure as an example (Fig. 6G) (*5*). Although modifying initial distribution of particles loaded in the syringe was found as an easy method for improving injectability, it might not always be feasible in clinical settings. Variations in initial particle distribution may make it challenging to control distribution of particles before the injections. Slow sedimentation velocity of small particles (<100 μm) can also make repositioning of particles a time-consuming process and hard for clinical translation.

As the second approach, we introduced design and manufacturing of a cost-effective fully mechanical syringe with an optimized profile at the tip inspired by pattern of streamlines and design of nozzles (Fig. 6, A to D). Specially designed syringe tip profile led to less dead volume, as a major driver of cost associated with medication waste (*37*), compared to the commercial syringe, and decreased particle loss (Fig. 6, E and F). Streamline-inspired syringe tip profile based on two interconnected nozzles contributed to enhanced flow of microparticles in the custom syringe and less particle accumulation in the corners. The proposed approach for design of the customized syringe based on conceptual and multiobjective optimization can be applicable to design of similar drug delivery devices such as needle-free injectors.

In this study, we used transparent resin (Formlabs Clear Resin) for stereolithography (SLA) 3D printing to better visualize flow of microparticles inside the syringe. While current 3D printing technologies can provide high-quality resolution and surface smoothness, for large-scale manufacturing, we envision that standard materials (e.g., polypropylene) and fabrication methods such as injection molding would be used. We further believe that the effect of material properties would be limited within a few debye lengths away from the inner wall (a few nanometers). Hence, material properties would not be expected to be of significance to the work presented here.

In summary, this study aimed to provide a comprehensive framework for microparticle injectability through hypodermic syringe needles and the techniques that can contribute to efficient microparticle delivery. Within the range of parameters studied, solution viscosity was found to be the statistically dominant factor followed by particle size and needle size. Increasing viscosity within the proposed range increased injectability. Increasing size of the particles and decreasing size of the needle in general decreased injectability. It was also found that concentrating particles in the centerline of the syringe, or with some offset from the plunger, can improve injectability. A mathematical formula was proposed to predict the chance of successful injection based on two nondimensional parameters, capturing properties of syringe, needle, and particles. The formula was further supplemented with an ANN, both indicating that a predicted injectability of 60% can be associated with actual injectability of more than 50%. A design framework based on numerical and experimental understanding helped manufacture a cost-effective syringe tailor-made for high injectability. The syringe provided higher delivery of microparticles as compared to a commercial syringe when administered subcutaneously to mice. Results of this study can potentially be used in a wide range of applications for parenteral injection of advanced drug delivery carriers and injectable biomaterials, especially subcutaneously, through conventional hypodermic needles, or design of novel drug delivery devices. Future efforts can be directed toward developing scalable, cost-effective microparticle-based drug delivery devices. Future follow-up studies could also be directed toward utilization of the proposed design platform to more deeply investigate how injectability could influence the therapeutic efficacy for different indications. A potential application of the current platform could be to decrease the frequency of injections by increasing deliverable payload per injection.

MATERIALS AND METHODS

Simulations

A multiphysics model was constructed in COMSOL Multiphysics version 5.2 (Burlington, MA) to numerically study particle transport in a syringe-needle system. The model coupled CFD with particle transport flow. Additional modification was applied to consider multiparticle clog formation at the needle inlet. Accordingly, particles within needle inlet would stick together and form a multiparticle clog if they were closer than a predefined distance R_c. The model was subsequently calibrated on the basis of experiments with similar boundary conditions to find the optimum R_c value for each needle size. In all simulations, solid microparticles were assigned a density of 1340 kg/m^3 to represent PLGA (L:G = 50:50). Particle transport simulations lasted for 12 s, equivalent to the time for complete plunger displacement in the corresponding experiments. The developed model was used to examine the effect of different design parameters on injectability including particle size, shape, concentration, initial distribution, needle size, and solution viscosity. Details of the modeling approach are provided in the Supplementary Materials.

Experiments

Rheometric test

Different viscosities were achieved by making different concentrations of MC (viscosity, 1500 cP; Sigma-Aldrich, USA) in water. Rheometric tests were performed at 20°C using a cup-and-bob geometry (fig. S5). The strain was held constant within the linear viscoelastic range. Subsequently, 16 data points were achieved by changing shear rate from 0.1 to 100 s^{-1}. Three different concentrations (w/v) of MC, including 1% MC (1% w/v MC), 2.5% MC, and 5% MC were studied. In this study, low- and high-viscosity solutions refer to 1% MC and 2.5% MC, respectively. Shear rate ($\dot{\gamma}$) was estimated using the following formula (*38*)

$$\dot{\gamma} = \frac{8v}{D} \quad (1)$$

where D is the inner diameter of the syringe and v is the plunger velocity (2.88 mm/s). The resulting shear rates for 1-ml and 3-ml syringes were within the same order of magnitude, and therefore, almost the same value of viscosity was measured for both syringes (fig. S5). The inner diameter (d) for 1-ml and 3-ml syringes were measured as 4.78 and 8.66 mm, respectively.

In vitro injection experiments

To conduct injection experiments in vitro, microparticles were collected and added to a 1.5-ml plastic tube containing about 300 μl of water. In vitro injection experiments were performed using an infusion syringe pump (Harvard Apparatus PHD ULTRA, USA) at a constant velocity of 2.88 mm/s. To retain a consistent plunger velocity identical for both syringes, different flow rates were used for each syringe size. Transferred particles were collected in a Petri dish and then counted multiple times using an optical microscope. Similarly, nontransferred microparticles remaining in the syringe/needle were counted at least three times under an optical microscope. The microparticle injectability percentage was calculated as the ratio of the number of transferred microparticles to Petri dish to the total number of microparticles initially loaded in the syringe. Hypodermic needles were purchased from BD, USA and TSK, Japan. All in vitro experiments were performed at least in triplicate. Highly concentrated microparticles were counted by image analysis using software ImageJ.

Design of experiments

We implemented a DOE approach to conduct the optimum number of required experiments necessary to systematically study and compare

the statistical significance of each design parameter. The statistical package Minitab was used to design the set of experiments on the basis of a Taguchi L_{18} orthogonal array. Design parameters studied included solution viscosity (i.e., polymer concentration), microparticle size, shape, concentration, and needle gauge. Different levels were considered for each parameter as tabulated in tables S2 and S3.

Subsequently, two different sets of DOEs were designed, namely, DOE1 and DOE2. In DOE1, viscosity was a variable, on the basis of making different concentrations of MC in water, including 0% (pure water), 1% (w/v), and 2.5% (w/v), and 16G, 18G, and 21G needles were considered. In DOE2, viscosity was constant at 1% MC, and needle sizes included 22G, 25G, and 30G. All experiments were performed for both a 1-ml and a 3-ml Luer-Lok syringe (18 experiments for each, $n = 3$ to 4), as a model syringe-needle system. A library of nine different microparticles was studied with full descriptions provided in table S1. Particles were classified into three size categories, namely, small, medium, and large. Statistical analysis was subsequently performed using Minitab statistical package. Results were analyzed using Taguchi mean of response and ANOVA to shed light on the relative ranking and significance of each design parameter on overall microparticle injectability.

Microfabrication and micromolding

To evaluate the effect of microparticle shape, spherical, cubic, and cylindrical microparticles were explored in this study. Spherical particles were purchased form Degradex, Phosphorex, USA, while nonspherical particles were manufactured using a micromolding technique fully described in (*5*). Unless otherwise stated, microparticles were made from PLGA (Resomer RG 502H; *L*:*G*, 50:50). PMMA and polystyrene microspheres were additionally investigated in some experiments. To compare microparticles with different shapes but similar size, microparticle volume was considered as the reference criterion for size. Full details of the microparticle used in the DOEs are provided in table S2. Scanning electron microscopy (SEM) was used to image particles. Samples were initially coated with a thin layer of Au/Pd using a Hummer 6.2 sputtering system (Anatech, Battle Creek, MI) and then imaged using a JSM-5600LV SEM (JEOL, Tokyo, Japan) with an acceleration voltage of 5 to 10 kV.

Statistical analysis

Pairwise statistical comparisons for in vitro and in vivo injection experiments were performed in GraphPad Prism (GraphPad Software, La Jolla, CA) using an ordinary one-way ANOVA with a Tukey multiple comparison test. Multivariable ANOVA in experimental section was performed in statistical package Minitab, USA. Statistical significance was considered for $P \leq 0.05$.

Predicting injectability and risk of needle blockage

Predicted injectability formula

To predict the effects of other parameter combinations on particle injectability, we aimed to model likely outcomes. A mathematical model based on a closed-form analytical solution can be extremely complicated because of the difficulty of solving hundreds of coupled temporospatial partial differential equations defining path lines for each particle. Inspired by Buckingham π theorem and the method of dimensional analysis, we proposed a model that uses two nondimensional parameters accounting for material properties and geometrical features to predict the chance of successful microparticle injection.

On the basis of finite element analysis and empirical studies, two types of forces were found to be highly decisive in microparticle injectability: particle density and viscous drag forces. To capture these effects, the following nondimensional parameter was introduced, representing particle and solution material properties defined as

$$\pi_1 = \frac{\mu}{\rho_p}\sqrt{\frac{C}{g}} \tag{2}$$

where μ is the viscosity of the solution at a given injection flow rate and C and ρ_p correspond to particle number concentration and particle density, respectively, while g is the gravitational acceleration. Furthermore, because of the strong effect of particle size and needle gauge on injectability, the ratio of the needle inner diameter (d_n) to the particle greatest dimension (d_p) was also incorporated into the model, yielding the second nondimensional parameter

$$\pi_2 = \frac{d_n}{d_p} \tag{3}$$

Subsequently, a general formula was proposed as follows

$$f(\pi_1, \pi_2) = a{\pi_1}^b + c{\pi_2}^d + e{\pi_1}^f{\pi_2}^g \tag{4}$$

in which the first two terms represent individual contribution and the last term represents interactive contributions of the two parameters, respectively. Curve fitting was performed using the Curve Fitting Toolbox in MATLAB to find the numerical constants noted as a to g in the proposed formula based on the results of DOEs. The resulting numerical coefficients a to g are tabulated in table S5, derived from curve fitting of Eq. 4 to the results of the experiments. This modeling approach provided an adjusted R^2 value of 0.74. An additional 22 validation experiments ($n = 3$) were also performed with at least one parameter deviating from the range investigated in the DOEs to further investigate prediction capability of the formula. The calculated predicted injectability values were subsequently compared and correlated with the actual experimental results (table S4).

Artificial neural network

An ANN was also used to provide a more sophisticated tool in addition to the proposed formula for predicting injectability based on the two dimensionless parameters previously described. The network structure was based on 10 hidden layers (fig. S4). Experiments, including both DOEs and validation sets, were incorporated into the network, each representing a single data point. As a result, 319 data points were incorporated into the network, 60% of which were specified to training, 20% to validation, and 20% to testing. The training was performed using the Levenberg-Marquardt backpropagation algorithm using the MATLAB Deep Learning Toolbox.

Design and manufacturing of a customized syringe

In this study, a new syringe was designed and manufactured to achieve high microparticle injectability with good cost effectiveness. Several steps were then taken toward design, optimization, manufacturing, and testing of the proposed model in vitro and in vivo. Briefly, a parametric numerical model was first developed to enhance average and maximum magnitude of the flow velocity at the syringe tip. A few prototypes were then manufactured on the basis of the optimized geometry out of around 500 designs. Injectability of microparticles was then compared to a commercial model, and the syringe with sufficient needle attachment and superior injectability in vitro was selected for in vivo subcutaneous injections to a mouse model. Detailed description of each step can be found in the Supplementary Materials.

SUPPLEMENTARY MATERIALS

Supplementary material for this article is available at http://advances.sciencemag.org/cgi/content/full/6/28/eabb6594/DC1

REFERENCES AND NOTES

1. R. Langer, New methods of drug delivery. *Science* **249**, 1527–1533 (1990).
2. R. Langer, Drug delivery and targeting. *Nature* **392**, 5–10 (1998).
3. K. E. Uhrich, S. M. Cannizzaro, R. S. Langer, K. M. Shakesheff, Polymeric systems for controlled drug release. *Chem. Rev.* **99**, 3181–3198 (1999).
4. D. A. Lavan, T. McGuire, R. Langer, Small-scale systems for in vivo drug delivery. *Nat. Biotechnol.* **21**, 1184–1191 (2003).
5. K. J. McHugh, T. D. Nguyen, A. R. Linehan, D. Yang, A. M. Behrens, S. Rose, Z. L. Tochka, S. Y. Tzeng, J. J. Norman, A. C. Anselmo, X. Xu, S. Tomasic, M. A. Taylor, J. Lu, R. Guarecuco, R. Langer, A. Jaklenec, Fabrication of fillable microparticles and other complex 3D microstructures. *Science* **357**, 1138–1142 (2017).
6. J. P. Rolland, B. W. Maynor, L. E. Euliss, A. E. Exner, G. M. Denison, J. M. DeSimone, Direct fabrication and harvesting of monodisperse, shape-specific nanobiomaterials. *J. Am. Chem. Soc.* **127**, 10096–10100 (2005).
7. S. Freiberg, X. X. Zhu, Polymer microspheres for controlled drug release. *Int. J. Pharm.* **282**, 1–18 (2004).
8. B. K. Kim, S. J. Hwang, J. B. Park, H. J. Park, Preparation and characterization of drug-loaded polymethacrylate microspheres by an emulsion solvent evaporation method. *J. Microencapsul.* **19**, 811–822 (2008).
9. A. Shamloo, M. Sarmadi, Z. Aghababaie, M. Vossoughi, Accelerated full-thickness wound healing via sustained bFGF delivery based on a PVA/chitosan/gelatin hydrogel incorporating PCL microspheres. *Int. J. Pharm.* **537**, 278–289 (2018).
10. J. A. Champion, Y. K. Katare, S. Mitragotri, Particle shape: A new design parameter for micro-and nanoscale drug delivery carriers. *J. Control. Release* **127**, 3–9 (2007).
11. P. L. Ritger, N. A. Peppas, A simple equation for description of solute release I. Fickian and non-fickian release from non-swellable devices in the form of slabs, spheres, cylinders or discs. *J. Control. Release* **5**, 23–36 (1987).
12. S. Mitragotri, P. A. Burke, R. Langer, Overcoming the challenges in administering biopharmaceuticals: Formulation and delivery strategies. *Nat. Rev. Drug Discov.* **13**, 655–672 (2014).
13. L. Arendt-Nielsen, H. Egekvist, P. Bjerring, Pain following controlled cutaneous insertion of needles with different diameters. *Somatosens. Mot. Res.* **23**, 37–43 (2006).
14. M. Iwanaga, K. Kamoi, Patient perceptions of injection pain and anxiety: A comparison of NovoFine 32-gauge tip 6mm and Micro Fine Plus 31-gauge 5mm needles. *Diabetes Technol. Ther.* **11**, 81–86 (2009).
15. F. Cilurzo, F. Selmin, P. Minghetti, M. Adami, E. Bertoni, S. Lauria, L. Montanari, Injectability evaluation: An open issue. *AAPS PharmSciTech* **12**, 604–609 (2011).
16. C. Berteau, O. Filipe-Santos, T. Wang, H. E. Rojas, C. Granger, F. Schwarzenbach, Evaluation of the impact of viscosity, injection volume, and injection flow rate on subcutaneous injection tolerance. *Med. Devices* **8**, 473–484 (2015).
17. E. L. Giudice, J. D. Campbell, Needle-free vaccine delivery. *Adv. Drug Deliv. Rev.* **58**, 68–89 (2006).
18. G. D. Chitnis, M. K. S. Verma, J. Lamazouade, M. Gonzalez-Andrades, K. Yang, A. Dergham, P. A. Jones, B. E. Mead, A. Cruzat, Z. Tong, K. Martyn, A. Solanki, N. Landon-Brace, J. M. Karp, A resistance-sensing mechanical injector for the precise delivery of liquids to target tissue. *Nat. Biomed. Eng.* **3**, 621–631 (2019).
19. J. A. Champion, S. Mitragotri, Role of target geometry in phagocytosis. *Proc. Natl. Acad. Sci. U.S.A.* **103**, 4930–4934 (2006).
20. J. A. Champion, A. Walker, S. Mitragotri, Role of particle size in phagocytosis of polymeric microspheres. *Pharm. Res.* **25**, 1815–1821 (2008).
21. M. Forouzandehmehr, A. Shamloo, Margination and adhesion of micro-and nanoparticles in the coronary circulation: A step towards optimised drug carrier design. *Biomech. Model. Mechanobiol.* **17**, 205–221 (2018).
22. T. Küme, A. R. Sişman, A. Solak, B. Tuğlu, B. Cinkooğlu, C. Coker, The effects of different syringe volume, needle size and sample volume on blood gas analysis in syringes washed with heparin. *Biochem. Med.* **22**, 189–201 (2012).
23. H. Zhong, G. Chan, Y. Hu, H. Hu, D. Ouyang, A comprehensive map of FDA-approved pharmaceutical products. *Pharmaceutics* **10**, 263 (2018).
24. A. Khalkhali, H. Noraie, M. Sarmadi, Sensitivity analysis and optimization of hot-stamping process of automotive components using analysis of variance and Taguchi technique. *Proc. Inst. Mech. Eng. Part E* **231**, 732–746 (2017).
25. R. D. Firouz-Abadi, H. Moshrefzadeh-Sany, H. Mohammadkhani, M. Sarmadi, A modified molecular structural mechanics model for the buckling analysis of single layer graphene sheet. *Solid State Commun.* **225**, 12–16 (2016).
26. M. H. Shojaeefard, A. Khalkhali, M. Sarmadi, N. Hamzehi, Investigation on the optimal simplified model of BIW structure using FEM. *Lat. Am. J. Solids Stru.* **12**, 1972–1990 (2015).
27. M. Sarmadi, A. Shamloo, M. Mohseni, Utilization of molecular dynamics simulation coupled with experimental assays to optimize biocompatibility of an electrospun PCL/PVA scaffold. *PLOS ONE* **12**, e0169451 (2017).
28. A. Shamloo, M. Sarmadi, Investigation of the adhesive characteristics of polymer–protein systems through molecular dynamics simulation and their relation to cell adhesion and proliferation. *Integr. Biol.* **8**, 1276–1295 (2016).
29. X. Luo, B. Yang, L. Sheng, J. Chen, H. Li, L. Xie, G. Chen, M. Yu, W. Guo, W. Tian, CAD based design sensitivity analysis and shape optimization of scaffolds for bio-root regeneration in swine. *Biomaterials* **57**, 59–72 (2015).
30. C. Rungsiyakull, Q. Li, G. Sun, W. Li, M. V. Swain, Surface morphology optimization for osseointegration of coated implants. *Biomaterials* **31**, 7196–7204 (2010).
31. W. Li, M. V. Swain, Q. Li, J. Ironside, G. P. Steven, Fibre reinforced composite dental bridge. Part II: Numerical investigation. *Biomaterials* **25**, 4995–5001 (2004).
32. M. O. Wang, C. E. Vorwald, M. L. Dreher, E. J. Mott, M.-H. Cheng, A. Cinar, H. Mehdizadeh, S. Somo, D. Dean, E. M. Brey, J. P. Fisher, Evaluating 3D-printed biomaterials as scaffolds for vascularized bone tissue engineering. *Adv. Mater.* **27**, 138–144 (2015).
33. M. Bohner, B. Gasser, G. Baroud, P. Heini, Theoretical and experimental model to describe the injection of a polymethylmethacrylate cement into a porous structure. *Biomaterials* **24**, 2721–2730 (2003).
34. M. S. Yeoman, D. Reddy, H. C. Bowles, D. Bezuidenhout, P. Zilla, T. Franz, A constitutive model for the warp-weft coupled non-linear behavior of knitted biomedical textiles. *Biomaterials* **31**, 8484–8493 (2010).
35. R. S. Rao, C. G. Kumar, R. S. Prakasham, P. J. Hobbs, The Taguchi methodology as a statistical tool for biotechnological applications: A critical appraisal. *Biotechnol. J.* **3**, 510–523 (2008).
36. K.-H. Yu, A. L. Beam, I. S. Kohane, Artificial intelligence in healthcare. *Nat. Biomed. Eng.* **2**, 719–731 (2018).
37. C. U. Oramasionwu, A. L. Cole, M. S. Dixon, S. J. Blalock, G. A. Zarkin, L. J. Dunlap, W. A. Zule, Estimated cost of injectable medication waste attributable to syringe dead space. *JAMA Intern. Med.* **176**, 1025–1027 (2016).
38. R. Darby, R. P. Chhabra, R. Darby, *Chemical Engineering Fluid Mechanics, Revised and Expanded* (CRC Press, 2001).
39. H. Wadell, Volume, shape, and roundness of quartz particles. *J. Geol.* **43**, 250–280 (1935).
40. X. Liu, L. H. Nielsen, S. N. Kłodzińska, H. M. Nielsen, H. Qu, L. P. Christensen, J. Rantanen, M. Yang, Ciprofloxacin-loaded sodium alginate/poly (lactic-co-glycolic acid) electrospun fibrous mats for wound healing. *Eur. J. Pharm. Biopharm.* **123**, 42–49 (2018).
41. O. Qutachi, J. R. Vetsch, D. Gill, H. Cox, D. J. Scurr, S. Hofmann, R. Müller, R. A. Quirk, K. M. Shakesheff, C. V. Rahman, Injectable and porous PLGA microspheres that form highly porous scaffolds at body temperature. *Acta Biomater.* **10**, 5090–5098 (2014).
42. T. W. J. Steele, C. L. Huanga, E. Widjaja, F. Y. C. Boey, J. S. C. Loo, S. S. Venkatramana, The effect of polyethylene glycol structure on paclitaxel drug release and mechanical properties of PLGA thin films. *Acta Biomater.* **7**, 1973–1983 (2011).
43. G. Chiandussi, M. Codegone, S. Ferrero, F. E. Varesio, Comparison of multi-objective optimization methodologies for engineering applications. *Comput. Math. Appl.* **63**, 912–942 (2012).

Acknowledgments: We would like to thank R. Farra, D. Brancazio, D. Chickering, and J. Webster for comments and feedback on this work. In addition, we acknowledge the MIT Department of Comparative Medicine for help in in vivo experiments, the Microsystems Technology Laboratories (MTL) for help in microfabrication process development, and S. Rose for help in micromolding. **Funding:** This work was supported by the Bill & Melinda Gates Foundation, Seattle, WA (OPP1095790). The animal facility used in this work is supported, in part, by the Koch Institute Support (core) Grant P30-CA14051 from the National Cancer Institute. Fellowship support for K.J.M. was supported by an NIH Ruth L. Kirschestein National Research Service Award (F32EB022416). **Author contributions:** M.S., A.M.B., and A. J. devised the concept of the study. M.S., A.M.B., and A.J. designed the experiments. M.S., H.T.M.C., Z.L.T., and K.J.M. performed the experiments, characterization, and imaging. M.S. performed statistical analysis and computational parts including simulations and modeling. M.S., R.L., K.J.M., A.M.B., X.L., and A.J. wrote, commented on, and reviewed the manuscript. R.L. and A.J. supervised the study. **Competing interests:** R.L., A.J., and K.J.M. are the holders of the patent describing fabrication

of core-shell microparticles titled "Micromolded or 3-D printed pulsatile release vaccine formulations" (U.S. patent application 10/300,136). K.J.M., A.J., and R.L. are the holders of another related patent titled "Microdevices with complex geometries," (filed 13 September 2017; application number US 62/558,172. For a list of entities with which R.L. is involved, compensated or uncompensated, see www.dropbox.com/s/yc3xqb5s8s94v7x/Rev%20Langer%20COI.pdf?dl=0 **Data and materials availability:** Raw data and codes used in this study can be provided upon reasonable request.

Submitted 9 March 2020
Accepted 22 May 2020
Published 8 July 2020
10.1126/sciadv.abb6594

Citation: M. Sarmadi, A. M. Behrens, K. J. McHugh, H. T. M. Contreras, Z. L. Tochka, X. Lu, R. Langer, A. Jaklenec, Modeling, design, and machine learning-based framework for optimal injectability of microparticle-based drug formulations. *Sci. Adv.* **6**, eabb6594 (2020).

ScienceAdvances

Modeling, design, and machine learning-based framework for optimal injectability of microparticle-based drug formulations

Morteza Sarmadi, Adam M. Behrens, Kevin J. McHugh, Hannah T. M. Contreras, Zachary L. Tochka, Xueguang Lu, Robert Langer, and Ana Jaklenec

Sci. Adv. **6** (28), eabb6594. DOI: 10.1126/sciadv.abb6594

Science Advances (ISSN 2375-2548) is published by the American Association for the Advancement of Science. 1200 New York Avenue NW, Washington, DC 20005. The title *Science Advances* is a registered trademark of AAAS.